

Oil Recovery from Micropatterned Triangular Troughs during a Surfactant Flood

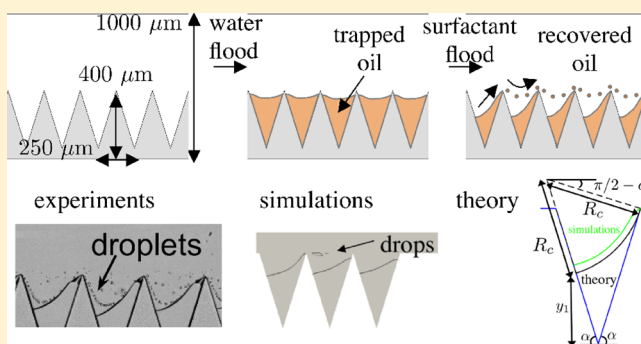
Ankur Gupta,^{†,§} Hyundo Lee,^{‡,§} and Patrick S. Doyle^{*,‡,§}

[†]Princeton University, 1 Olden Street, Princeton, New Jersey 08544, United States

[‡]Massachusetts Institute of Technology, E17-504F, 77 Mass Avenue, Cambridge, Massachusetts 02139, United States

Supporting Information

ABSTRACT: We study the recovery of oil trapped inside micropatterned triangular troughs after injecting a surfactant solution. In our experiments, we track the trapped oil volume with duration of surfactant flood for different capillary numbers. We observe that the capillary number affects the amount of oil recovered as well as the rate of oil recovery. We employ multiphase flow simulations to analyze our system and show a qualitative agreement between the simulations and experimental results. We also discover that beyond a capillary number, the volume of oil recovered plateaus, and no additional oil is released with an increase in capillary number. We develop a theoretical model to predict the dependence of maximum oil recovery on geometrical features and find that the theoretical predictions compare favorably with the trends obtained from our simulations. Though approximate, theoretical relation provides insights into the efficiency of oil recovery and can be utilized to understand the effect of sharp bends and dead ends in enhanced oil recovery and soil remediation.



INTRODUCTION

Enhanced oil recovery (EOR) and nonaqueous phase liquid (NAPL) recovery from underground water resources commonly utilize surfactant solutions for mobilization of oil or pollutants.^{1–4} It is well-established that surfactants are effective because they alter the wetting properties of the liquid–solid interface and reduce the interfacial tension between the liquid phases.^{5–8} However, because classical techniques such as core flooding and packed beds cannot be utilized for direct flow visualization, the effect of pore morphology in these processes is relatively less explored. Thus, micromodels or two-dimensional (2-D) structures designed for flow visualization in porous media are gaining importance in the literature.^{9,10} For instance, 2-D cylindrical micromodels have been utilized to investigate the formation of bridges, formation of thin films,¹¹ spreading of liquid jet,¹² and fluid displacement using foams.¹³ In addition, pore-throat micromodels have been utilized for lab-on-chip reservoir studies.^{14–16} Though these studies provide important insights into flow patterns within a reservoir, the complicated geometry of micromodels makes it challenging to parse the physical processes.

In this study, we build upon our previously developed micromodel approach that provides full control over designing geometrical features with tailored wetting properties.¹⁷ We also showed that by controlling the geometry of photopatterned obstacles and sidewalls, a water flood can be utilized to trap oil in varying amounts.^{18,19} Here, we use the same approach to trap the oil phase in triangular patterned structures. Next, we

examine the release of entrapped oil through a surfactant flood. More specifically, we focus on the effect of capillary number on oil recovery. We also perform multiphase flow simulations to investigate the physical mechanism of oil recovery. Last, we also comment on the effect of amplitude and frequency of triangular troughs, which is useful to understand the role of sharp bends, dead ends, and tortuous paths inside a pore.

We note that though the primary motivation of this work is EOR and NAPL, our results are also of potential use in the field of liquid-infused patterned surfaces—or microtextured surfaces with a precoating of a liquid that demonstrate remarkable properties such as hydrophobicity and antifouling—where this work will help understand the removal of the existing liquid layer.^{20–27} Recently, a series of studies examined the removal of a liquid layer from micropatterned grooves.^{24–27} However, these studies did not consider variation in the shape of geometric features.

MATERIALS AND METHODS

Materials. Acrylated glass microchannels are products of Hilgenberg GmbH. Polyurethane acrylate MINS 311RM (precursor) is a product of Minuta Tech. 2-Hydroxy-2-methylpropiophenone (photoinitiator), tetramethylpiperidinyloxy (terminator), *n*-decane (oil), and sodium dodecyl sulphate (SDS) are products of Sigma-

Received: June 25, 2018

Revised: August 16, 2018

Published: August 20, 2018

Aldrich. Deionized water is used in all experiments. A syringe pump from Harvard apparatus is used for injecting liquids in the microchannel.

Experimental Details. We use a glass microchannel with dimensions length $L = 18$ mm (x), width $W = 1$ mm (y), and height $H = 50$ μm (z) (Figure 1a). We fill the channel with a mixture of

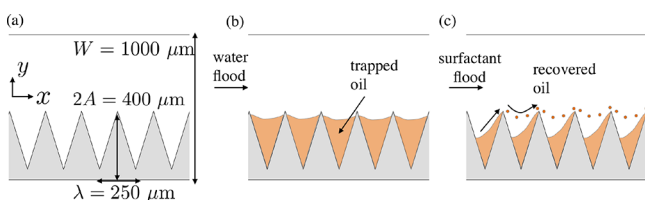


Figure 1. Schematic of the setup. (a) Triangular pattern of amplitude 400 μm and wavelength 250 μm is photopatterned in a glass microchannel of width 1000 μm and height 50 μm . (b) First, the channel is filled with oil. Next, the oil is trapped in triangular troughs with a water flood. (c) Post oil entrapment, a surfactant flood is carried out at different flow rates to recover the trapped oil.

precursor, 5% (v/v) photoinitiator, and 0.1% (w/w) terminator. We photopattern a triangular structure at one of the sidewalls using the projection lithography method.^{17,18,28–32} The triangular pattern is created with amplitude of $2A = 400$ μm and wavelength of $\lambda = 250$ μm . First, we fill the channel with oil (decane). Next, we displace the oil by injecting water at speed $U = 4$ mm/s. As water flows inside the microchannel, oil is trapped in the triangular troughs because of wetting and geometric effects (Figure 1b). We refer the readers to our previous work, where we analyze the oil displacement process and predict the amount of oil entrapped using geometric arguments.¹⁹ After the oil entrapment step, we flood the channel with 5 wt % SDS solution with speed varying from $U = 9$ –700 mm/s to recover the trapped oil (Figure 1c).

Simulation Details. We use a multiphase volume of fluid (VOF) method to analyze our system. We assume oil as the first phase with properties ρ_o (density of oil), μ_o (viscosity of oil), and surfactant solution as the second phase with the physical properties similar to water, that is, ρ_w (density of water) and μ_w (viscosity of water). The interfacial tension between the two phases is defined as σ . The VOF method introduces a variable ϕ , which is the volume fraction of the oil phase. Volume fraction is the probability of finding the oil phase at a specific location and thus $0 \leq \phi \leq 1$. Because the method assumes ϕ as a continuous variable, values between 0 and 1 are also possible, leading to a diffuse interface. VOF defines the global ρ and μ as follows

$$\rho = \rho_o \phi + \rho_w (1 - \phi) \quad (1)$$

$$\mu = \mu_o \phi + \mu_w (1 - \phi) \quad (2)$$

The method solves for the volume fraction ϕ , velocity field \vec{u} , and pressure P through the following equations

$$\nabla \cdot \vec{u} = 0 \quad (3)$$

$$\frac{\partial \phi}{\partial t} + \vec{u} \cdot \nabla \phi = 0 \quad (4)$$

$$\rho \left(\frac{\partial \vec{u}}{\partial t} + (\vec{u} \cdot \nabla) \vec{u} \right) = -\nabla P + \nabla \cdot (\mu S) + f \quad (5)$$

$$f = \sigma k \frac{2\rho}{\rho_o + \rho_w} \nabla \phi \quad (6)$$

$$k = -\nabla \cdot \hat{n} \quad (7)$$

$$\hat{n} = \frac{\nabla \phi}{|\nabla \phi|} \quad (8)$$

$$S_{ij} = \frac{1}{2} \left(\frac{\partial u_j}{\partial x_i} + \frac{\partial u_i}{\partial x_j} \right) \quad (9)$$

Equations 3 and 4 are expressions for total mass balance and phase mass balance, respectively. Equation 5 is the momentum conservation equation with an additional force f that takes into account the interfacial force. f is calculated through eq 6 and depends on the curvature k , which in turn depends on ϕ , as shown in eqs 7 and 8. The contact line is captured in simulations through the parameter k as it includes the gradient of ϕ . Furthermore, a vanishing gradient of ϕ implies a flat interface or a contact angle of $\theta = 90^\circ$, where θ is the contact angle of oil in water. We estimate $\rho_w = 10^3$ kg/m³, $\mu_w = 10^{-3}$ Pa·s, $\mu_o = 10^{-3}$ Pa·s, and $\sigma = 6 \times 10^{-3}$ N/m.

Finite volume software openFoam is used for all computational calculations. The utility *blockMesh* is used to construct and mesh a three-dimensional geometry that comprises of three triangular troughs. A uniform meshing grid is used with a typical cell size of 12.5 μm . Velocity inlet and pressure outlet conditions are used for inlet and outlet faces, respectively, and a no-slip condition is used for the walls. A contact angle of $\theta = 90^\circ$ is implemented at the walls by assuming a zero gradient for ϕ (see eqs 7 and 8). We note that in experiments, the modified sidewalls show a contact angle of $\theta = 35^\circ$ before the surfactant flood¹⁹ and a contact angle of $\theta = 93^\circ$ after the surfactant is introduced (calculated using microscopic images). To simplify the numerical calculations, we assume $\theta = 90^\circ$ because it implies a vanishing gradient of ϕ . The VOF equations are solved using the utility *interFoam*. We note that we have not included the effect of contact angle dynamics, that is, the effect of θ on Ca , because it is significantly more challenging to include this effect reliably in VOF simulations.

RESULTS AND DISCUSSION

The main focus of this work is to estimate the effect of surfactant solution flow rate on oil recovery. We define U as the average velocity of the surfactant solution which varies from 9 to 700 mm/s. Changing U affects capillary number $Ca = \frac{\mu_w U}{\sigma} = 1.5 \times 10^{-3} - 1.16 \times 10^{-1}$ as well as Reynolds number $Re = \frac{\rho_w U H}{\mu_w} = 0.45 - 35$. However, for the same capillary number, change in Re does not affect the release, as discussed in our prior work.¹⁹ For simplicity, we do not vary the viscosity ratio μ_o/μ_w , which also affects this system.¹⁹ Therefore, the critical dimensionless number here is Ca .

We define dimensionless volume V as the ratio of oil volume trapped inside the trough to the volume of a trough. V prior to surfactant flood is taken to be V_0 . Intuitively, one expects to see an improvement in oil recovery with increase in Ca . We observe a similar behavior in our experiments (Figure 2). The

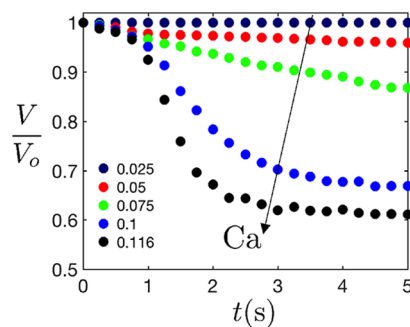


Figure 2. Experimental results. Evolution of trapped oil volume for different Ca . V is defined as the ratio of volume of oil inside a trough to the volume of trough. V is V_0 at $t = 0$.

trends suggest that for $Ca \leq 0.025$, there is practically no oil recovery. However, as Ca number increases, a larger amount of oil is released. Also, we find that the rate of recovery is different for different Ca with the volume of trapped oil becoming relatively constant after 5 s.

We discover that there are two modes of oil release mechanism, a slow mode and a fast mode. During the slow mode, the recovery is relatively mild as only a few droplets of oil are released intermittently. Here, first the interface deforms and the contact line moves upward to the top right corner of the triangular trough (Figure 3a, see Supporting Information

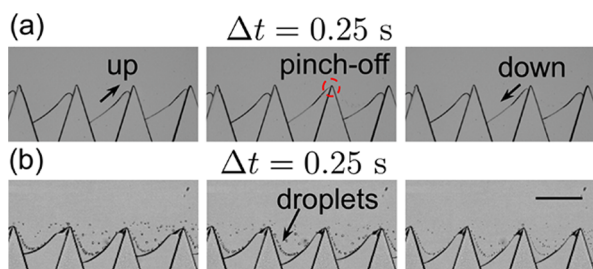


Figure 3. Modes of oil recovery. (a) During the slow mode, the interface deforms and the contact line moves up the right wall until it reaches the top right corner. Afterward, the oil droplet pinches-off and the contact line slides down. This cycle is repeated such that oil droplets are released in a “pulsating” fashion. Slow mode is observed for low Ca or for late times for high Ca . (b) Fast recovery phase is characterized by a continuous stream of droplets. This mode is only observed for higher Ca . The scale bar is $250 \mu\text{m}$.

Videos 1 and 3). Afterward, a few droplets are released and the contact line retracts. The slow mode has a typical “pulsating” behavior, where the droplets are released periodically. We believe that this process is reminiscent to a tip streaming process, wherein the surfactant is swept to the tip of the interface, thereby reducing the interfacial tension and creating droplets.³³ Droplet generation in turn decreases the surfactant concentration on the interface, and the process repeats once enough surfactant accumulates onto the fresh interface. The slow mode is observed for low Ca or near saturation for high Ca .

In the fast mode, a continuous stream of droplets is generated while the contact line is pinned at the top right corner of the trough (Figure 3b), see Supporting Information Videos 1 and 3. We observe that the released droplets do not coalesce with the oil trapped downstream. This occurs because of the repulsive interaction between the surfactant molecules. Microscopic images suggest that the released droplet size is on

the order of $d \approx 10 \mu\text{m}$. Assuming a critical capillary number between $Ca_{\text{crit}} = 0.1\text{--}0.2$,³⁴ we estimate the droplet size by balancing interfacial stress (σ/d) and shear stress ($\frac{3\mu_w U}{H}$) or $d = \frac{Ca_{\text{crit}} \sigma}{\left(\frac{3\mu_w U}{H}\right)} = 14\text{--}28 \mu\text{m}$, which is in reasonable agreement with the experimental values.

In the experimental results discussed above, Ca was increased by changing the flow rate of the surfactant solution. We note that it is also possible to change Ca by changing the surfactant concentration but that would also influence the interfacial tension. Therefore, we did not vary this parameter in the experiments. However, this could be a focus of future studies in this area.

To gain a better understanding of our experimental findings, we perform multiphase flow simulations. Figure 4 summarizes the results obtained from simulations. We define dimensionless time $\tilde{t} = \frac{tU}{w}$. The trends for V/V_0 from simulations display qualitative similarities with experiments. For instance, there is an improvement in the amount of oil recovered with increase in Ca . The trends show that there is no recovery for $Ca \leq 0.025$. Moreover, the rate of recovery depends on Ca (\tilde{t} is scaled by average velocity U). In addition, we see a saturation in trapped volume for long flooding times. Quantitatively, for high Ca , the volume of oil trapped for long times is similar to experiments.

There are also important differences between experiments and simulation findings. In the simulations, we find that the released oil coalesces with the oil trapped in downstream troughs ($\tilde{t} = 1.14, 1.65$, see Supporting Information Videos 2 and 4) because we do not consider the repulsive interactions between the surfactant molecules (the results of V/V_0 in Figure 4 are thus plotted only for the left-most trough to exclude the effect of coalescence). Also, though the kinetic variation of V/V_0 is qualitatively similar, the time scales differ by almost 2 to 3 orders of magnitude. $\tilde{t} = 10$ corresponds to $t = 0.014$ s, whereas we observe changes on the order of a few seconds in experiments. We also do not observe intermittent or pulsating droplet generation. We attribute the above discrepancies to the lack of surfactant transport in our simulations. In the actual experiments, the interface is initially free of surfactants, and there is a time scale associated with the surfactant transport to the interface. In contrast, in the simulations, we set Ca by the equilibrium interfacial tension, thereby predicting a much shorter time scale of droplet breakup. Several studies have theoretically discussed the effect of surfactant transport during droplet deformation.^{33,35,36} Unfortunately, the theoretical equations discussed in these reports are not compatible with

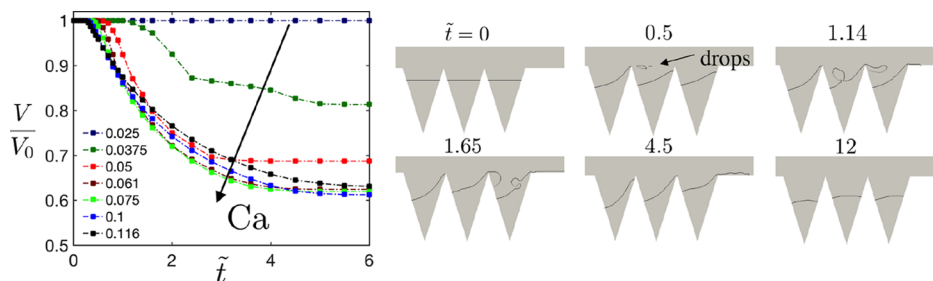


Figure 4. Summary of results from simulation. Evolution of trapped oil volume for different Ca (left). We define $\tilde{t} = \frac{tU}{w}$. Representative snapshots of contours of $\phi = 0.5$ from simulations (right).

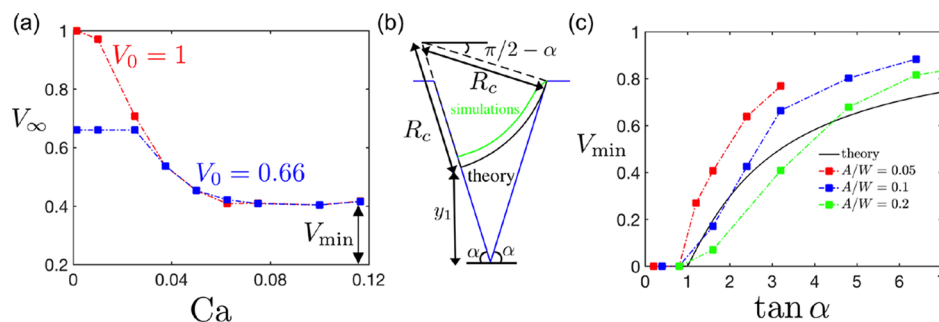


Figure 5. Geometrical effects. Variation of the final trapped oil volume V_∞ with Ca for different V_0 obtained from simulations. We define V_{\min} as the oil volume that is not recovered even at high Ca . (b) Theoretical setup to predict dependence of V_{\min} . We approximate the interface before the contact line slides down the top right corner as a circular arc. The circular arc touches the right triangular corner and is normal to the left edge. The theoretical prediction for interface shows reasonable agreement with the simulation contour for $\phi = 0.5$ (results shown for $A = 200 \mu\text{m}$, $\lambda = 250 \mu\text{m}$). (c) Effect of geometry on V_{\min} .

the VOF framework and are thus beyond the scope of this work. However, previous studies help us understand the pulsating mechanism of droplet generation, that is, surfactant convects and accumulates toward the tip of the droplet leading to a droplet breakup. Once the droplet breaks, the process repeats itself once enough surfactant reaccumulates on the fresh interface.

A key prediction of our simulations is that the volume of oil trapped at long times, V_∞ , becomes relatively independent of Ca , see Figure 4. Physically, this result implies that beyond a Ca , V_∞ does not decrease further because the surfactant is unable to push additional oil out from the trough. Because of experimental limitations, we were unable to reach beyond $Ca = 0.116$ and could not verify this result experimentally. However, this result is not unexpected because a similar observation is common in core flooding experiments where a portion of oil is believed to be stuck in dead end pores and is never recovered. To confirm this hypothesis further, we varied V_0 in our simulations and observed that V_∞ is independent of V_0 at large Ca (Figure 5a, Supporting Information Video 5), suggesting that geometry plays a dominant role in dictating maximum possible recovery. We define V_∞ at large Ca as V_{\min} , and thus, $1 - V_{\min}$ is a measure of maximum oil recovery for a given geometry.

To provide an estimate of V_{\min} , we argue that the recovery of oil stops when the interface is unable to reach the top right corner (see Supporting Information Videos 1–5). To predict this critical condition theoretically, we assume a circular interface that is normal to the left edge of the triangle and that touches the top right corner. The value of the contact angle $\theta = 90^\circ$ is implicitly assumed because the interface is set to be normal to the solid surface. To include the effect of contact angle, one can modify the angle at which the interface intersects the left wall. We note that the assumption of the interface as a circular arc is not strictly valid because shear forces are not negligible when compared to interfacial forces. However, because the velocity magnitudes in the trough are smaller than the bulk of the microchannel, it is a reasonable first-order approximation. In the simulations, at the critical condition, the interface changes its curvature near the top right corner and becomes parallel to the flow direction (see Supporting Information Video 2). However, the change in curvature is currently ignored for simplicity. The trough angle α satisfies $\tan \alpha = \frac{4A}{\lambda}$, where A is the amplitude and λ is the wavelength, see Figures 1 and 5. Further, we define y_1 as the

vertical height of the contact line at the left wall and R_c as the radius of the assumed circular arc (see Figure 5). On the basis of these assumptions, we can write the following geometrical equations

$$y_1 + R_c \sin \alpha = 2A + R_c \cos \alpha \quad (10)$$

$$R_c \cos \alpha + \frac{y_1}{\tan \alpha} + \frac{\lambda}{2} = R_c \sin \alpha \quad (11)$$

Upon simplification of eqs 10 and 11, we obtain

$$y_1 = 2A \tan(\alpha - \pi/4) \quad (12)$$

We note that an arc constructed through this geometrical model is in good agreement with the contour obtained from simulations, see Figure 5b. This shows that our assumption of a circular interface arc is reasonable to predict the criterion for maximum oil recovery. Furthermore, because the theoretical profile does not capture the bending of the interface near the right corner, the theoretical prediction would underestimate the amount of remaining entrapped oil and overestimate the maximum oil recovery. To estimate V_{\min} , we calculate the volume of the prism formed by the ends of the circular arc or

$$V_{\min} \approx \frac{\frac{1}{2} \times y_1 \times \frac{2A}{\sin \alpha} \times \sin(\pi - 2\alpha) \times HW}{A\lambda H} \approx \sin \alpha \tan(\alpha - \pi/4) \quad (13)$$

We present the predictions of eq 13 in Figure 5c and compare them with simulations. We find that theoretical calculations yield a qualitatively similar trend where there is complete recovery for $\tan \alpha \leq 1$. Further, V_{\min} increases with increase in $\tan \alpha$ or the recovery is lower with increase in slope. However, the simulations predict a dependence on A/W unlike our geometrical model. This discrepancy occurs because the theory neglects the effect of difference in flow patterns for different values of A/W . Nonetheless, eq 13 provides a quick and easy way to predict the amount of oil recovery possible for different geometries. For instance, for $\tan(\alpha) = 3.2$ used in experiments, eq 13 predicts $V_{\min} = 0.5$. From Figure 2, we find that at $Ca = 0.116$, $V_\infty = 0.61$, which is reasonably close to our prediction from geometrical calculations, especially because we expect the theoretical prediction to underestimate the amount of entrapped oil. We emphasize that $1 - V_{\min}$ is a measure of maximum oil recovery. For $\alpha = \pi/3$ and $\alpha = \frac{5\pi}{12}$, $1 - V_{\min}$ is estimated to be 0.77 and 0.44, respectively. Therefore, a

modest increase in α leads to a drastic reduction in oil recovery. Further, for $\alpha = \pi/2$, $1 - V_{\min} = 0$ or no oil is recovered, consistent with expectation. We note that though the actual geometries might not be as simple as a triangular trough, a global slope of the geometry can be used as $\tan \alpha$ in eq 13 to get a first-order estimate.

CONCLUSIONS

In this article, we experimentally and theoretically investigate the release of trapped oil from a triangular trough during a surfactant flood. Our experiments show that the final recovery as well as the rate of recovery depends on capillary number Ca . Our simulations capture some of the experimentally observed features but deviate quantitatively because the simulations ignore surfactant transport to the interface. We discover that oil recovery saturates at large capillary numbers because of geometrical constraints. Last, we provide a simple equation to approximately predict maximum oil recovery.

We believe our work is of importance in EOR and NAPL. Equation 13, albeit approximate, provides a quick way to estimate maximum oil recovery. This result can be used to investigate the effects of dead ends, sharp bends, and tortuosity of the pores and provides a way to account for the effects of spatial permeability in fundamental multiphase flow modeling.^{37,38} Our analysis also provides information about limits for failure of liquid-infused surfaces. For instance, we report that oil recovery starts to occur around $Ca \approx 0.1$, providing a rationale for choosing chemicals for liquid coating. Last, our work can be used for deciding the shape of fibers, printing surfaces, and patterned surfaces.^{39–43}

ASSOCIATED CONTENT

Supporting Information

The Supporting Information is available free of charge on the ACS Publications website at DOI: 10.1021/acs.langmuir.8b02150.

Details of supplementary videos (PDF)

Experimental oil release mechanism result under conditions $A = 200 \mu\text{m}$, $\lambda = 250 \mu\text{m}$, and $U = 700 \text{ mm/s}$ for 5 wt % SDS flood; simulation result under conditions $A = 200 \mu\text{m}$, $\lambda = 250 \mu\text{m}$, and $U = 700 \text{ mm/s}$ for 5 wt % SDS flood; experimental oil release mechanism result under conditions $A = 200 \mu\text{m}$, $\lambda = 250 \mu\text{m}$, and $U = 450 \text{ mm/s}$ for 5 wt % SDS flood; simulation result under conditions $A = 200 \mu\text{m}$, $\lambda = 250 \mu\text{m}$, and $U = 225 \text{ mm/s}$ for 5 wt % SDS flood; and simulation result under conditions $A = 200 \mu\text{m}$, $\lambda = 250 \mu\text{m}$, $U = 700 \text{ mm/s}$ for 5 wt % SDS flood (ZIP)

AUTHOR INFORMATION

Corresponding Author

*E-mail: pdoyle@mit.edu.

ORCID

Ankur Gupta: 0000-0003-3474-9522

Patrick S. Doyle: 0000-0003-2147-9172

Author Contributions

§A.G. and H.L. contributed equally to this work.

Notes

The authors declare no competing financial interest.

ACKNOWLEDGMENTS

A.G. and H.L. contributed equally to this work. A.G. acknowledges the financial support from Hugh Hampton Young Fellowship. H.L. acknowledges the funding from Samsung Fellowship.

REFERENCES

- (1) Sheng, J. *Modern Chemical Enhanced Oil Recovery: Theory and Practice*; Gulf Professional Publishing, 2010.
- (2) Babadagli, T. Evaluation of the critical parameters in oil recovery from fractured chalks by surfactant injection. *J. Pet. Sci. Eng.* **2006**, *54*, 43–54.
- (3) Hirasaki, G. J.; Miller, C. A.; Puerto, M. Recent advances in surfactant EOR. *SPE Annual Technical Conference and Exhibition*, 2008, conference proceeding.
- (4) Mulligan, C.; Yong, R.; Gibbs, B. Surfactant-enhanced remediation of contaminated soil: a review. *Eng. Geol.* **2001**, *60*, 371–380.
- (5) Standnes, D. C.; Austad, T. Wettability alteration in chalk: 2. Mechanism for wettability alteration from oil-wet to water-wet using surfactants. *J. Pet. Sci. Eng.* **2000**, *28*, 123–143.
- (6) Standnes, D. C.; Austad, T. Wettability alteration in carbonates: interaction between cationic surfactant and carboxylates as a key factor in wettability alteration from oil-wet to water-wet conditions. *Colloids Surf., A* **2003**, *216*, 243–259.
- (7) Wu, Y.; Shuler, P. J.; Blanco, M.; Tang, Y.; Goddard, W. A. An experimental study of wetting behavior and surfactant EOR in carbonates with model compounds. *SPE J.* **2008**, *13*, 26–34.
- (8) Fletcher, P. D.; Savory, L. D.; Woods, F.; Clarke, A.; Howe, A. M. Model study of enhanced oil recovery by flooding with aqueous surfactant solution and comparison with theory. *Langmuir* **2015**, *31*, 3076–3085.
- (9) Karadimitriou, N. K.; Hassanizadeh, S. A review of micromodels and their use in two-phase flow studies. *Vadose Zone J.* **2012**, *11*, vzj2011.0072.
- (10) Sinton, D. Energy: the microfluidic frontier. *Lab Chip* **2014**, *14*, 3127–3134.
- (11) Grate, J. W.; Zhang, C.; Wietsma, T. W.; Warner, M. G.; Anheier, N. C.; Bernacki, B. E.; Orr, G.; Oostrom, M. A note on the visualization of wetting film structures and a nonwetting immiscible fluid in a pore network micromodel using a solvatochromic dye. *Water Resour. Res.* **2010**, *46*, W11602.
- (12) Horgue, P.; Augier, F.; Duru, P.; Prat, M.; Quintard, M. Experimental and numerical study of two-phase flows in arrays of cylinders. *Chem. Eng. Sci.* **2013**, *102*, 335–345.
- (13) Conn, C. A.; Ma, K.; Hirasaki, G. J.; Biswal, S. L. Visualizing oil displacement with foam in a microfluidic device with permeability contrast. *Lab Chip* **2014**, *14*, 3968–3977.
- (14) Gunda, N. S. K.; Bera, B.; Karadimitriou, N. K.; Mitra, S. K.; Hassanizadeh, S. M. Reservoir-on-a-Chip (ROC): A new paradigm in reservoir engineering. *Lab Chip* **2011**, *11*, 3785–3792.
- (15) Schneider, M. H.; Tabeling, P. Lab-on-chip methodology in the energy industry: wettability patterns and their impact on fluid displacement in oil reservoir models. *Am. J. Appl. Sci.* **2011**, *8*, 927.
- (16) Wu, M.; Xiao, F.; Johnson-Paben, R. M.; Retterer, S. T.; Yin, X.; Neeves, K. B. Single-and two-phase flow in microfluidic porous media analogs based on Voronoi tessellation. *Lab Chip* **2012**, *12*, 253–261.
- (17) Lee, H.; Lee, S. G.; Doyle, P. S. Photopatterned oil-reservoir micromodels with tailored wetting properties. *Lab Chip* **2015**, *15*, 3047–3055.
- (18) Lee, H.; Gupta, A.; Hatton, T. A.; Doyle, P. S. Creating isolated liquid compartments using photopatterned obstacles in microfluidics. *Phys. Rev. Appl.* **2017**, *7*, 044013.
- (19) Gupta, A.; Lee, H.; Doyle, P. S. Controlled liquid entrapment over patterned sidewalls in confined geometries. *Phys. Rev. Fluids* **2017**, *2*, 094007.

- (20) Wong, T.-S.; Kang, S. H.; Tang, S. K.; Smythe, E. J.; Hatton, B. D.; Grinthal, A.; Aizenberg, J. Bioinspired self-repairing slippery surfaces with pressure-stable omniphobicity. *Nature* **2011**, *477*, 443–447.
- (21) Lafuma, A.; Quéré, D. Slippery pre-suffused surfaces. *Europhys. Lett.* **2011**, *96*, 56001.
- (22) Smith, J. D.; Dhiman, R.; Anand, S.; Reza-Garduno, E.; Cohen, R. E.; McKinley, G. H.; Varanasi, K. K. Droplet mobility on lubricant-impregnated surfaces. *Soft Matter* **2013**, *9*, 1772–1780.
- (23) Epstein, A. K.; Wong, T.-S.; Belisle, R. A.; Boggs, E. M.; Aizenberg, J. Liquid-infused structured surfaces with exceptional anti-biofouling performance. *Proc. Natl. Acad. Sci. U.S.A.* **2012**, *109*, 13182–13187.
- (24) Wexler, J. S.; Grosskopf, A.; Chow, M.; Fan, Y.; Jacobi, I.; Stone, H. A. Robust liquid-infused surfaces through patterned wettability. *Soft Matter* **2015**, *11*, 5023–5029.
- (25) Wexler, J. S.; Jacobi, I.; Stone, H. A. Shear-driven failure of liquid-infused surfaces. *Phys. Rev. Lett.* **2015**, *114*, 168301.
- (26) Jacobi, I.; Wexler, J. S.; Stone, H. A. Overflow cascades in liquid-infused substrates. *Phys. Fluids* **2015**, *27*, 082101.
- (27) Liu, Y.; Wexler, J. S.; Schönecker, C.; Stone, H. A. Effect of viscosity ratio on the shear-driven failure of liquid-infused surfaces. *Phys. Rev. Fluids* **2016**, *1*, 074003.
- (28) Lee, H.; Srinivas, R. L.; Gupta, A.; Doyle, P. S. Sensitive and multiplexed on-chip microRNA profiling in oil-isolated hydrogel chambers. *Angew. Chem.* **2015**, *127*, 2507–2511.
- (29) Dendukuri, D.; Pregibon, D. C.; Collins, J.; Hatton, T. A.; Doyle, P. S. Continuous-flow lithography for high-throughput microparticle synthesis. *Nat. Mater.* **2006**, *5*, 365–369.
- (30) Dendukuri, D.; Gu, S. S.; Pregibon, D. C.; Hatton, T. A.; Doyle, P. S. Stop-flow lithography in a microfluidic device. *Lab Chip* **2007**, *7*, 818–828.
- (31) Bong, K. W.; Bong, K. T.; Pregibon, D. C.; Doyle, P. S. Hydrodynamic focusing lithography. *Angew. Chem., Int. Ed.* **2010**, *49*, 87–90.
- (32) Chapin, S. C.; Appleyard, D. C.; Pregibon, D. C.; Doyle, P. S. Rapid microRNA profiling on encoded gel microparticles. *Angew. Chem., Int. Ed.* **2011**, *50*, 2289–2293.
- (33) Eggleton, C. D.; Tsai, T.-M.; Stebe, K. J. Tip streaming from a drop in the presence of surfactants. *Phys. Rev. Lett.* **2001**, *87*, 048302.
- (34) Stone, H. A. Dynamics of drop deformation and breakup in viscous fluids. *Annu. Rev. Fluid Mech.* **1994**, *26*, 65–102.
- (35) Stone, H. A.; Leal, L. G. The effects of surfactants on drop deformation and breakup. *J. Fluid Mech.* **1990**, *220*, 161–186.
- (36) Anna, S. L. Droplets and bubbles in microfluidic devices. *Annu. Rev. Fluid Mech.* **2016**, *48*, 285–309.
- (37) Cueto-Felgueroso, L.; Juanes, R. A phase-field model of two-phase Hele-Shaw flow. *J. Fluid Mech.* **2014**, *758*, 522–552.
- (38) Cueto-Felgueroso, L.; Juanes, R. Macroscopic phase-field model of partial wetting: bubbles in a capillary tube. *Phys. Rev. Lett.* **2012**, *108*, 144502.
- (39) Protiere, S.; Duprat, C.; Stone, H. A. Wetting on two parallel fibers: drop to column transitions. *Soft Matter* **2013**, *9*, 271–276.
- (40) Sauret, A.; Boulogne, F.; Cébron, D.; Dressaire, E.; Stone, H. A. Wetting morphologies on an array of fibers of different radii. *Soft Matter* **2015**, *11*, 4034–4040.
- (41) Patel, R.; Benkreira, H. Gravure roll coating of Newtonian liquids. *Chem. Eng. Sci.* **1991**, *46*, 751–756.
- (42) Chung, C.; Kumar, S. Emptying of viscoelastic liquids from model gravure cells. *J. Non-Newtonian Fluid Mech.* **2015**, *221*, 1–8.
- (43) Huang, C.-H.; Carvalho, M. S.; Kumar, S. Stretching liquid bridges with moving contact lines: comparison of liquid-transfer predictions and experiments. *Soft Matter* **2016**, *12*, 7457–7469.